THE JOURNAL OF PHYSICAL CHEMISTRY C

Article

pubs.acs.org/JPCC

On Asymmetric Surface Barriers in MFI Zeolites Revealed by Frequency Response

Andrew R. Teixeira,[§,†] Xiaoduo Qi,[§,†] Chun-Chih Chang,[†] Wei Fan,[†] Wm. Curtis Conner,[†] and Paul J. Dauenhauer*[,†,‡]

[†]Department of Chemical Engineering, University of Massachusetts Amherst, 686 North Pleasant Street, Amherst, Massachusetts 01003, United States

[‡]Department of Chemical Engineering and Materials Science, University of Minnesota, 421 Washington Ave. SE, Minneapolis, Minnesota 55455-0132, United States

Supporting Information

ABSTRACT: Diffusional mass transport in porous materials is important for shape-selective catalysis and separation technologies. To maximize turnover and catalytic site accessibility, hierarchical materials are synthesized with length scales as small as single crystal lattices (~2 nm, MFI). While these materials are potentially efficient catalysts, they have been shown to exhibit apparent diffusivities that are orders of magnitude slower than those in bulk crystals. To evaluate the dependence of apparent diffusivity with particle size, the kinetics and mechanism have been characterized by frequency response methods for cyclohexane mass transfer into and out of silicalite-1 particles varying in size over two orders of magnitude. Development of a new mass transport model utilizes data obtained by frequency response to characterize two sequential rate limitations: intracrystalline diffusion and asymmetric surface barriers. Activation energy associated with transport into the surface ($E_{a,s}$ = 20.8 kJ/mol) was observed to be significantly less than that of intracrystalline diffusion and release (E_a = 53.9 kJ/mol ≈ 54.1 kJ/mol = $E_{a,-s}$). Surface pore blockages are proposed to dominate mass transport in small zeolite particles.

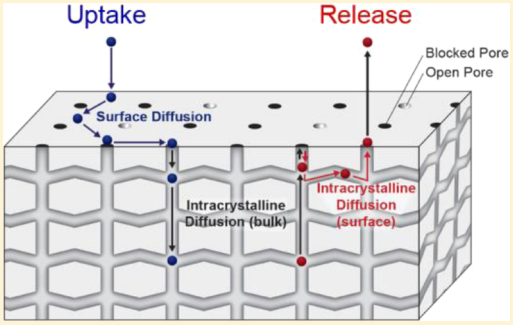

1.0. INTRODUCTION

Zeolites are broadly utilized to catalyze chemical reactions to improve selectivity to desired products through well-ordered, shape-selective microporous channels.[1] For catalytic reactions in microporous materials, reactants undergo a number of sequential transient processes including adsorption, diffusion, and surface reactions.[2] For large zeolite particles, the apparent (experimentally determined) turnover frequency is limited by the rate of mass transfer because of slow diffusion in long pores. To reduce mass transfer limitations, nanoscale zeolites have been synthesized with diffusional length scales several orders of magnitude smaller than those of large, crystalline zeolite particles,[3,4] introducing new capabilities for fast reaction and separation applications.

Within the new class of micro- and mesoporous materials, zeolites are now being synthesized with length scales approaching that of a single unit cell (pillared,[5,6] nanosheets,[7] membranes,[8−10] etc.). These hierarchical structures build on micropores (well-ordered lattice structures, ~2 nm) with mesopores (ordered or disordered pore networks, 2−50 nm) and macropores (interstitial particle voids, > 50 nm). For example, 3DOm-i zeolites are synthesized using a carbon template to create MFI-structured particles only 35 nm in size; close-packing produces a hierarchical structure with well-defined mesopores (6−9 nm), and the whole particle is generated at radii as large as 1 μm.[3,4] Additionally, pentasil structures consist of MFI sheets only one or two unit cells thick, with mesopores of 3−7 nm within particle radii as large as 100 nm.[4,11]

New mesoporous zeolite structures with microcrystalline domains below 20 nm are dominated by their surfaces, making characterization and/or prediction of their physical and chemical properties difficult. Recent characterization by zero-length chromatography of cyclohexane transport in MFI-structured 3DOm-i has shown that hierarchical, mesoporous materials provide overall mass transfer faster than that of larger single crystals,[3] as expected. However, the benefit of smaller crystalline domains was not as fast as expected; shorter transport length scales did not result in *predictably* faster transport time scales.[4] Additional characterization by zero-length chromatography of cyclohexane transport in MFI has also shown that particle surfaces contribute significantly to the overall rate of transport as particles become smaller.[10] Apparent diffusivity determined by experiment of mesoporous zeolite materials comprises two parts (surface and bulk transport), resulting in values of apparent diffusivity that vary by as much as three orders of magnitude as particles vary in size between 20 nm and 3 μm.[12] Moving forward, it is paramount to understand transport limitations of

Received: July 18, 2014
Revised: September 1, 2014
Published: September 2, 2014

   dx.doi.org/10.1021/jp507212b | J. Phys. Chem. C 2014, 118, 22166−22180

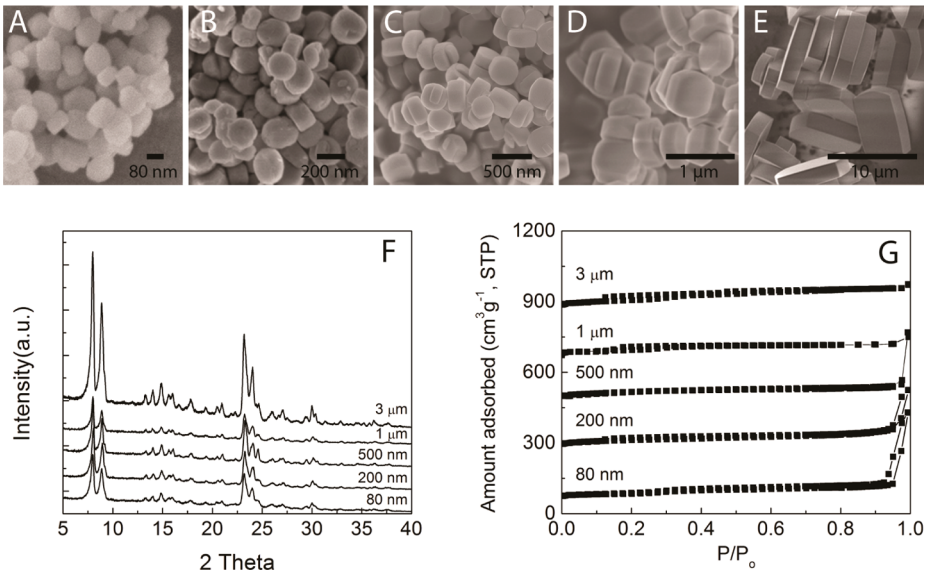

Figure 1. Characterization of zeolite particles. (A) SEM micrographs show monodisperse particles of "coffin" geometry for the five particles examined in this study. (B) XRD data show the scattering patterns and high level of crystallinity typical of purely MFI structured zeolites. (C) N_2 adsorption isotherms exhibit a purely microporous regime for all particles.

both bulk diffusion and diffusion through the surface for design and utilization of these novel zeolitic materials.

Characterization of diffusion in porous zeolite materials requires knowledge of the characteristic length scales of particles and the type of mass transport. While bulk gas-phase diffusion (adsorbate−adsorbate interactions) in large pores is fast, mass transfer slows within mesopores as guest−host interactions occur more frequently and Knudsen diffusion dominates as diffusivity becomes a function of pore diameter at low pressures.[10,11] As the pore diameter is further decreased comparable to the kinetic diameter of the adsorbate (guest molecule), diffusion is characterized by the configurational diffusion regime and the rate of diffusion is governed by a series of adsorption steps and molecule reorientation.[10,11] In some cases, the existence of systems with both small mesopores and small microcrystalline domains has led to rate-controlling transport in both the micropores and mesopores.[13] This complication is avoided in this experimental study (this paper) by (a) selection of purely microporous MFI-structured zeolites (silicalite-1; pore size, 5.5−6 Å[14]) and (b) selection of a slow-diffusing adsorbate, cyclohexane (critical molecular diameter, 6.8 Å[14]), such that diffusion through the bulk of zeolites are shown to be solely configurational diffusion.[4] For these conditions, temperature-activated diffusion coefficients obtained from experimental methods, D_{app}, represent the rate coefficients associated with the rate-limiting elementary step of moving from one stable site to an adjacent stable site within the microporous zeolite framework. In the case of the bulk crystal, this coefficient is characteristic of the intracrystalline diffusivity (D) and is temperature-activated in accordance with the Arrhenius relationship (E_a).

While bulk mass transport in zeolites is widely studied, little is known with regard to fundamental understanding of transport at or near the surface of zeolites.[15,16] It is understood that additional transport limitations beyond bulk particle diffusion must be considered because of internal grain boundaries and defects,[17−19] surface adsorption−desorption,[20,21] and most recently the possibility of structural defects at the surface causing partial or total pore blockages.[12,22,23] The contributions of these potential secondary mass transfer limitations have been probed by several experimental techniques that have been developed to study diffusion in microporous materials.[24,25] The techniques are classified as either equilibrium measurements (pulsed field gradient nuclear magnetic resonance (PFG-NMR),[26] tracer zero-length column (tracer-ZLC)[27]) or transport measurements (frequency response,[28] ZLC,[12] gravimetric[29,30]), where the two sets of measured diffusivities are not identical. Equilibrium techniques measure the self-diffusivity (or tracer diffusivity) under equilibrium conditions, whereas transport techniques measure the transport diffusivity (or apparent diffusivity) in the presence of concentration gradients. The two values can be related by the Darken relationship, which accounts for different loadings by describing the transport diffusivity (D_{app}) as being proportional to the self-diffusivity (D_s) with the proportionality factor being the local slope of the adsorption isotherm.[31,32] Despite the wide array of experimental techniques and thermodynamic correction factors, differences in observed diffusion coefficients have been reported to vary by as many as three orders of magnitude for different techniques.[15,16] Recently, the same trend was also observed by the use of a single technique and attributed to the strong size-dependence of the apparent diffusion coefficient, leading to the conclusion that transport limitations at or near the surface (surface barriers) dominate the observed mass transport in small zeolite particles.[4,12]

In this work, we evaluate the relative contributions to mass transfer of cyclohexane in a range of silicalite-1 particle sizes using frequency response. Experimental data collected over a range of particle sizes and temperatures are compared with the existing base model for adsorbate diffusion as well as the Yasuda surface resistance model,[33] which accounts for desorption rate limitations at the surface. A new model is developed to account for the surface limitation which allows for different kinetics between uptake and release (i.e., bidirectional) of adsorbates through the surface. Deconvoluting the kinetics of bulk diffusion from the surface barrier for both uptake into the pores and release of the pores provides the first mechanistic insight (e.g., kinetic energy barriers) into the nature of MFI surface barriers.

dx.doi.org/10.1021/jp507212b | J. Phys. Chem. C 2014, 118, 22166−22180

2.0. METHODS

Silicalite-1 particles were synthesized and characterized as described previously.[12,34] In short, tetrapropylammonium hydroxide (TPAOH) solutions, tetraethylorthosilicate (TEOS), and water were combined and aged at 353 K for 1 day while being continuously stirred. The gel composition was set with SiO_2 = 0.25, and stoichiometric ratios of TPAOH to water of 11, 28, 100, and 400 for the 80 nm, 200 nm, 500 nm, and 1 μm samples, respectively. The gel was then heated at 443 K for 1 day, then washed and centrifuged until the supernatant pH fell below 9. The largest sample (3 μm) was synthesized by a slightly different method,[12,35] aging tetrapropylammonium bromide (TPABr) and NaOH at 323 K for 8 days first. The gel was formed with the composition SiO_2:0.1 TPABr:0.05 Na_2O:4 EtOH:98 H_2O, which was then heated in an autoclave at 408 K for 50 h before being washed thoroughly with deionized water and dried at 373 K overnight.

Particle size distributions and morphologies were determined using a Magellan 400 (FEI) or 6320JXV (JEOL) to perform scanning electron microscopy (SEM; Figure 1A–E and Table 1).

Table 1. Physical Dimensions of Silicalite-1 Particles

nominal crystal size	length (nm)	width (nm)	height (nm)	R (nm)[a]
3 μm	7680	4120	1550	1800
1 μm	1110	730	420	430
500 nm	460	460	256	231
200 nm	190	170	90	88
80 nm	80	60	60	42.3

[a] R is calculated according to

$$R = \sqrt[3]{\frac{(LWH)3}{4\pi}}$$

Samples were prepared on a carbon tape then coated with Pt before being scanned. Acceleration voltages of 3.0 kV with a stage bias of 500 V were used. In all cases, particle size distributions were narrow, validating the monodisperse synthesis.

X-ray diffraction (XRD) was performed on a 'Pert Pro by PANalytical with Cu Kα radiation. For all crystal sizes, characteristic reflections from MFI were observed (Figure 1F) without indication of crystalline impurities, confirming the crystallinity and structure of silicalite-1. Nitrogen adsorption isotherms were obtained on an Autosorb iQ by Quantachrome. Samples were outgassed at 473 K until pressure changes were observed below 25 mTorr/min. Isotherms were collected at 77 K (Figure 1G) and shown to exhibit the large microporous regime typical of MFI for all particles. Micropore volumes calculated by the t-plot method were all in the range of 0.10–0.13 cm^3/g, indicating the high expected range for purely MFI structured material.

2.1. Frequency Response Apparatus. The frequency response (FR) method was first established by Yasuda to investigate adsorption[36] then later diffusion of guest sorbates into porous materials.[37] In this method, the pressure response of a closed sorption chamber under periodic volume perturbations with different frequencies is recorded and fit to a theoretical adsorption–diffusion model. Because of the wide range of the perturbation frequencies available, the frequency response method is able to measure diffusion coefficients that span several orders of magnitude.

A schematic diagram of the frequency response apparatus is presented in Figure 2 and described in detail by Turner et al.[28]

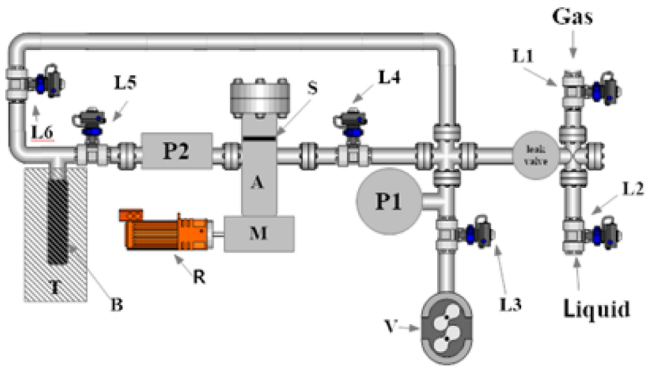

Figure 2. Schematic depicting the experimental frequency response apparatus for measuring diffusion in zeolites. A sinusoidal volume change is induced in the sample chamber, and the corresponding pressure response is fit to coupled particle–chamber mass balances.

The analytical apparatus is composed of a servomotor (R), bellows pump, sample chamber (A), rapid differential pressure transducer (P), dosing manifold, vacuum system (V), and data acquisition system. The servomotor (R) is equipped with an integrated proportional–integral–derivative (PID) controller which allows control of the position and speed of the motor shaft in the range of 0.001–40 Hz. A bellows pump is placed between the motor (R) and the sorption chamber (A) and is used to drive the sinusoidal volume change. The sample chamber (A) is a 316 stainless 4-way cross with a supported stage and imbedded thermocouple. Copper sealed flanges are used to maintain high vacuum (10^{-6} to 10^{-8} Torr) inside the chamber. The total volume (neutral bellow displacement) of the camber is 584 cm^3, while the bellows can displace ±2% of the total volume. The chamber is maintained at isothermal temperatures (set to 50 < T < 275 °C) by performing PID control on three band heaters located around the entire chamber and allowing sufficient time for thermal equilibration. The sample size (bed thickness) is maintained sufficiently small such that no temperature or pressure gradients exist across the bed. The pressure transducer (P2) on the sorption chamber (A) is a MKS Baratron 10 Torr differential capacitance manometer. The transducer is fixed to the sorption chamber (A) and then referenced to a 150 cm^3 ballast (B). The ballast is housed in an isothermal water bath (T) to maintain constant reference pressure. The dosing manifold comprises a stainless steel four-way cross and a three-way tee with a total volume of 270 cm^3. Two inlets (L1, L2) are fixed to the dosing manifold and allow for dosing of either a constant pressure gaseous adsorbate from the upper inlet (L1) or a known partial vapor pressure liquid adsorbate from the lower port (L2). The entire system is equipped with an ultrahigh vacuum pumping system (V) to allow for complete pump-down prior to dosing. The vacuum system (V) consists of a rotary rough pump and turbo-molecular pump which allows for evacuation to 10^{-8} Torr.

2.2. Frequency Response Experiment. Five monodisperse silicalite-1 samples of particles varying over three orders of magnitude in size were synthesized and characterized,[12] as summarized in Table 1. Figure 1 shows the scanning electron micrographs, X-ray diffraction, and nitrogen adsorption isotherms for all silicalite-1 samples used in this study. Although all zeolite samples exhibited the "coffin" geometry, the three-

dx.doi.org/10.1021/jp507212b | J. Phys. Chem. C 2014, 118, 22166–22180

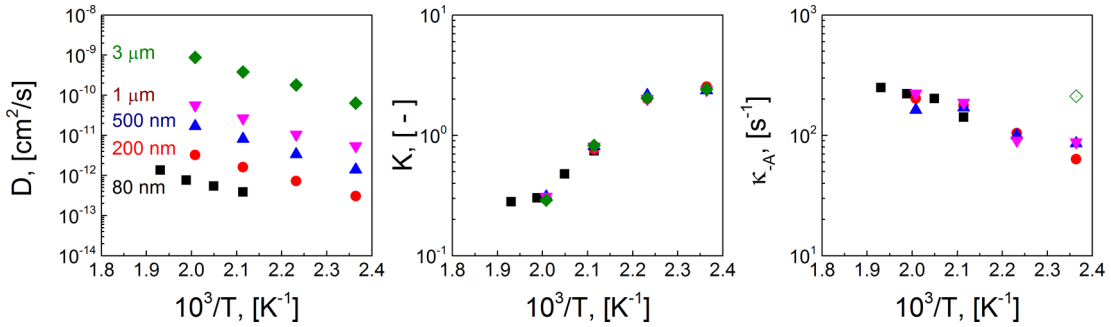

Figure 3. Yasuda surface resistance model. The Yasuda surface resistance model fit was performed independently at each particle size and temperature. While the equilibrium constant and surface barrier parameter collapse for all particles, significant size-dependence is observed in the diffusion coefficient, indicating that the Langmuir resistance does not accurately capture the observed surface barriers here.

dimensional nature of the MFI pore network makes a spherical geometry more representative for diffusion analysis in small particles, as has previously been shown.[12,38]

Prior to each run, zeolite samples (150 mg) were degassed inside the sorption chamber overnight at 373 K and 10^{-8} Torr. The sorbate (cyclohexane, previously degassed by the "freeze–pump–thaw" method) was then introduced to the sorption chamber at a constant partial pressure through a leak valve, and the sorbate/sorbent system was allowed to reach equilibrium at the desired pressure. A sine-wave volume perturbation of 2% was then applied to the chamber, and an online data acquisition system recorded the transient pressure response from the pressure transducer. For larger zeolite samples (3 μm, 1 μm), a frequency range of 0.0025–10 Hz was scanned over 28 steps. For smaller zeolite samples (500 nm, 200 nm, 80 nm), a frequency range of 0.01–10 Hz was scanned over 23 steps.

The range of measurable particle sizes analyzed in the frequency response apparatus was considered to ensure measurable mass transport. The diffusional time constant must fall within the measurable transport time range such that the corner frequency (the peak of the out-of-phase function, described in section 3.0) is within the experimental frequency bounds (0.0025–10 Hz for the present system). For this reason, larger particles require the frequency range to be extended. Similarly, the range of diffusivities being examined are at relatively high temperatures compared to those used in previous study by ZLC to ensure operation in the proper regime.[12] For the diffusion-controlled case, the lower and upper limits of the particle size can be validated by substituting the frequency range and diffusion coefficient into $f = D/R^2$. While this criteria is met for the large particle base case ($D/R^2 \sim 10^{-3}$ s^{-1}), the apparent transport time scale no longer scales with the particle size in small particles. Specifically, the transport limitations examined in this study shift the apparent diffusivity to lower values, causing the corner frequency to fall within experimental limits; thus, this criterion is achieved (Figure 3).

3.0. FREQUENCY RESPONSE THEORY

As presented in Figure 4, several models have been proposed in the literature to describe mass transport between gases and solids. Each model describes the rate-limited transport phenomena that results in macroscopically observed mass transfer rates. In this study, experimental data were fit to three models: (i) a base model describing intracrystalline diffusion, (ii) Yasuda's surface resistance model which adds a surface adsorption–desorption limitation, and (iii) a new model which allows for an asymmetric surface barrier (model IV in Figure 4).

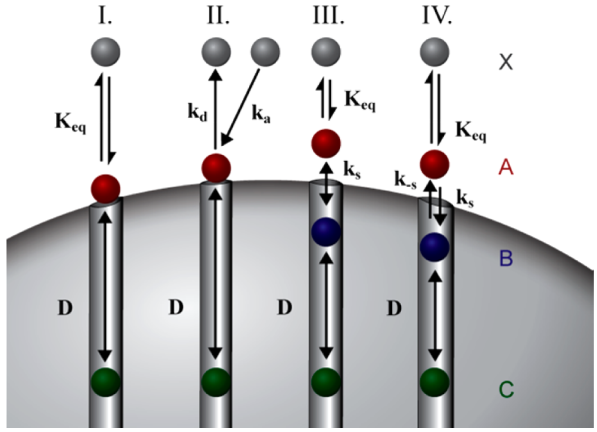

Figure 4. Schematic representation of four zeolite mass transport models. (I) Base case, (II) Yasuda surface resistance, (III) Ruthven surface barrier, and (IV) Teixeira–Qi asymmetric surface barrier.

The first frequency response model was derived by Yasuda to study the adsorption–desorption of gas molecules onto nonporous metal oxide surfaces.[36] The derivation was based on the Taylor series expansion of the general adsorption–desorption rate equation ($R_j = R_{j,e} + (\partial R_j/\partial P)(P - P_e) + (\partial R_j/\partial A)(A - A_e)$) and the mass balance within the entire chamber. The kinetics of the adsorption–desorption steps are described by Langmuir kinetics as[33,39]

$$\frac{d}{dt}N = k_j P(N_s - N) - k_{-j}N = -(k_j P + k_{-j})N + k_j P N_s \quad (1)$$

Because the volume and pressure of the system are changing with time, the theoretical model was expressed in terms of real (in-phase) and imaginary (out-of-phase) parts as shown below.

$$\frac{v}{p}\sin\phi = \sum_j \frac{k_j \omega}{k_{-j}^2 + \omega^2} \quad (2)$$

$$\frac{v}{p}\cos\phi - 1 = \sum_j \frac{k_j k_{-j}}{k_{-j}^2 + \omega^2} \quad (3)$$

where the Langmuir adsorption and desorption rate constants are respectively defined as

$$k_j = \frac{RT}{V_e}\left(\frac{\partial R_j}{\partial P}\right)_e \quad (4)$$

dx.doi.org/10.1021/jp507212b | J. Phys. Chem. C 2014, 118, 22166–22180

$$k_{-j} = -\left(\frac{\partial R_j}{\partial A_j}\right)_e \tag{5}$$

R_j is the adsorption rate of species j. A_j is the amount of surface species j. The phase lag of the pressure response is represented by $\varphi = \varphi_z - \varphi_b$, where φ_z and φ_b are the phase lags measured with and without sorbent, respectively. The amplitude ratio of the volume displacement (v) is assessed in the absence of sorbent, and the pressure amplitude ratio (p) is observed with the sorbent in response to the volume change.

3.1. Model I: Base Case. The adsorption−desorption model was modified by Yasuda to investigate the diffusion process within zeolites (Figure 4, model I).[40,41] In this case, the rates of surface adsorption and desorption are assumed to be infinite, implying the overall process is controlled by intracrystalline diffusion. Analytical solutions of in-phase and out-of-phase are derived in the section C2 of the Supporting Information. The functions were derived by combining Fick's first and second laws (diffusion in the pores), Henry's law (equilibrium at the surface), and the overall mass balance in the chamber. For a diffusion process occurring within a spherical zeolite, the two characteristic functions for the in-phase (eq 6) and out-of-phase (eq 7) are as follows:

$$\frac{v}{p}\sin\phi = K\delta_s = \frac{6K}{\eta'}\left[\frac{1}{2}\left(\frac{\sinh\eta' + \sin\eta'}{\cosh\eta - \cos\eta'}\right) - \frac{1}{\eta'}\right] \tag{6}$$

$$\frac{v}{p}\cos\phi - 1 = K\delta_C = \frac{K}{\eta'}\left\{\frac{\sinh\eta' + \sin\eta'}{\cosh\eta' + \cos\eta'}\right\} \tag{7}$$

where

$$\eta' = \sqrt{\frac{2\omega R^2}{D}}, \qquad K = \frac{RTV_S}{V_e}K_H \tag{8}$$

V_S is the volume of the zeolite, V_e the equilibrium volume of the chamber, and K_H Henry's law constant. R is the particle radius, and D is the intracrystalline diffusion coefficient.

3.2. Model II: Yasuda Surface Resistance. Yasuda extended the base model to describe the case in which rates of adsorption and desorption on the surface are not infinite (Figure 4, model II). In this surface resistance model, the kinetic contribution to the rate exists in accordance with traditional Langmuir adsorption−desorption kinetics (eq 1) such that the time scale for adsorption−desorption may contribute significantly to the overall transport time.[40,41] In this case, in-phase and out-of-phase functions are

$$\delta_S^{SR} = \left(\frac{a\kappa_a}{\omega}\right)\left[1 - \left(\frac{ak_a}{\omega}\right)\left\{\frac{\frac{a\kappa_a}{\omega} + c\delta_s}{\bar{\theta}}\right\}\right] \tag{9}$$

$$\delta_c^{SR} = \left(\frac{a\kappa_a}{\omega}\right)^2\left\{\frac{a + c\delta_c}{\bar{\theta}}\right\} \tag{10}$$

where δ_c and δ_s and the in-phase and out-of-phase functions described for the base case, and

$$\bar{\theta} = \left[\left(\frac{a\kappa_a}{\omega}\right) + c\delta_s\right]^2 + (a + c\delta_c)^2 \tag{11}$$

$$a = \left(\frac{dA}{dP}\right)_e\left(\frac{d(A + C)}{dP}\right)_e^{-1} = 1 - c \tag{12}$$

In eq 12, A represents the amount of species on the surface and C is that within the pores. From the definition of the Langmuir isotherm at the surface (eq 1), κ_a is the sum of adsorption and desorption rate constants ($\kappa_a = k_aP + k_d$). The parameter $a\kappa_a$ physically represents the inverse time scale of surface resistance. The magnitude of the surface barrier effect can be inferred from the area to the right of the intersection between in-phase and out-phase function curves. Mathematically, the magnitude of the cross area depends on the value of dimensionless number (λ), which characterizes the ratio of diffusion time scale to surface resistance time scale

$$\lambda = \frac{\tau_D}{\tau_s} = a\kappa_a\frac{R^2}{D} \tag{13}$$

3.3. Model IV: Teixeira−Qi (T-Q). The surface-barrier model derived by Yasuda assumes that the rates of mass transfer into and out of the surface are related to equilibrium by the Langmuir relationship (eq 1). While this model accurately describes the situation in which surface barriers arise from adsorption−desorption limitations, it does not describe the other mechanisms for surface barriers (pore narrowing, pore blockage). Ruthven previously removed the Langmuir constraint in lieu of a lumped *symmetrical* barrier at the surface for the desorption case (Figure 4, model III).[42] However, the Ruthven model does not extend to the combined uptake and release system in which separate rates (*asymmetric*) into and out of the surface may be observed. Because of these limitations, a new surface-barrier model with two surface rate constants (forward and reverse) is derived to improve upon the previous surface restriction. In this model, the following assumptions are made:

1. Diffusion inside the zeolite is assumed to be Fickian.
2. The diffusion coefficient and surface rate parameters are solely functions of temperature and are independent of concentration (valid for dilute systems) and particle size.
3. Periodic volume perturbation is small (<2%).
4. The total surface concentration (C_R) is the sum of the outer surface concentration A and inner surface concentration B, both evaluated at $r = R$.

The governing mass balance within a spherical zeolite particle can be expressed as

$$\frac{\partial C}{\partial t} = \frac{D}{r^2}\frac{\partial}{\partial r}\left\{r^2\frac{\partial C}{\partial r}\right\} \tag{14}$$

At the center of the zeolite, the symmetry boundary condition is

$$\left.\frac{\partial C}{\partial r}\right|_{r=0} = 0 \tag{15}$$

The boundary condition at the surface arises by balancing the internal flux (Fickian) with the flux through the surface. In this case, the flux at the surface is described as the sum of the rates into and out of the surface

$$J_s = \frac{R}{3}[k_sA - k_{-s}B] \tag{16}$$

where J_s is the surface flux, k_{-s} the rate constant associated with release from the surface, and k_s the uptake rate constant. A is in

dx.doi.org/10.1021/jp507212b | J. Phys. Chem. C 2014, 118, 22166−22180

Table 2. Frequency Response Parameters Obtained from Fitting Models I (Base), II (Yasuda), and IV (Teixeira−Qi)

	I. base case[a]			II. Yasuda surface resistance			IV. T-Q bidirectional surface resistance[b]			
	T (K)	D ($\times 10^{12}$ cm^2/s)	K (−)	D ($\times 10^{12}$ cm^2/s)	K (−)	κ_{-A} (s^{-1})	D ($\times 10^{12}$ cm^2/s)	K (−)	k_s (s^{-1})	k_{-s} (s^{-1})
3 μm	423	62.6	2.40	63.8	2.42	212.0	0.14	7.35	0.19	0.0026
	448	168	2.03	181.7	2.05	–	0.28	6.22	0.30	0.0053
	473	376	0.83	381.8	0.83	–	0.50	2.45	0.35	0.0128
	498	741	0.30	886.1	0.29	–	1.10	0.91	0.49	0.0244
1 μm	423	–	–	5.43	2.39	87.7	0.14	7.35	0.19	0.0026
	448	–	–	10.61	2.02	90.8	0.28	6.22	0.30	0.0053
	473	–	–	26.92	0.81	188.1	0.50	2.45	0.35	0.0128
	498	–	–	56.78	0.31	223.1	1.10	0.91	0.49	0.0244
500 nm	423	–	–	1.39	2.37	85.8	0.14	7.35	0.19	0.0026
	448	–	–	3.39	2.17	100.3	0.28	6.22	0.30	0.0053
	473	–	–	8.16	0.81	170.5	0.50	2.45	0.35	0.0128
	498	–	–	17.02	0.31	163.2	1.10	0.91	0.49	0.0244
200 nm	423	–	–	0.31	2.54	63.5	0.14	7.35	0.19	0.0026
	448	–	–	0.72	2.02	104.5	0.28	6.22	0.30	0.0053
	473	–	–	1.61	0.77	177.0	0.50	2.45	0.35	0.0128
	498	–	–	3.23	0.30	203.0	1.10	0.91	0.49	0.0244
80 nm	473	–	–	0.39	0.74	141.7	–	–	–	–
	488	–	–	0.55	0.48	202.1	–	–	–	–
	503	–	–	0.77	0.30	221.7	–	–	–	–
	518	–	–	1.36	0.28	249.4	–	–	–	–

[a]Fit obtainable only for largest particle. [b]Model optimization was performed over entire particle size domain such that only one set of parameters exists at each temperature.

equilibrium with the gas in accordance with Henry's Law. When assumptions 3 and 4 are applied, eq 16 becomes

$$J_s = k_s\frac{R}{3}C_R - (k_{-s} + k_s)\frac{R}{3}\frac{k_s}{k_{-s}}A \tag{17}$$

This surface flux has to be balanced with the diffusion flux giving rise to the second boundary condition

$$\left.\frac{dC}{dr}\right|_R = \frac{-R}{3D}\left[k_s(C_R - C_{R,e}) - (k_{-s} + k_s)\frac{k_s}{k_{-s}}\left(\frac{K_H}{V_s}(P - P_e)\right)\right] \tag{18}$$

where $K_H = d(V_sA)/dP$ is the local Henry's constant. The above boundary value problem can be further nondimensionalised as follows:

$$\frac{\lambda}{1+\lambda}\frac{\partial\bar{C}}{\partial\tau} = \frac{1}{\eta^2}\frac{\partial}{\partial\eta}\left(\eta^2\frac{\partial\bar{C}}{\partial\eta}\right) \tag{19}$$

with boundary conditions,

$$\left.\frac{d\bar{C}}{d\eta}\right|_{\eta=0} = 0 \tag{20}$$

$$\left.\frac{d\bar{C}}{d\eta}\right|_{\eta=1} = -\frac{R^2}{3D}k_s(\bar{C} - \bar{P}) \tag{21}$$

where,

$$\eta \equiv \frac{r}{R}$$

$$\tau \equiv \frac{t}{t_D + t_S} = \frac{t}{\frac{R^2}{D} + \frac{1}{k_s + k_{-s}}} = \frac{Dt}{R^2}\left(1 + \frac{1}{\lambda}\right)^{-1}$$

$$\lambda \equiv \frac{t_D}{t_s} = \left(\frac{D}{R^2}\frac{1}{k_s + k_{-s}}\right)^{-1}$$

$$\bar{C} \equiv \frac{C - C_e}{C_e} \tag{22}$$

The above boundary value problem can be solved by using Laplace transform and the resulting concentration profile is

$$\tilde{C} = \frac{1}{\eta}\left[\frac{R^2}{3D}k_s\tilde{P}\sinh\frac{\sqrt{\frac{\lambda}{1+\lambda}s}\,\eta}{\left[-\sinh\left(\sqrt{\frac{\lambda}{1+\lambda}s}\right) + \sqrt{\frac{\lambda}{1+\lambda}s}\cosh\left(\sqrt{\frac{\lambda}{1+\lambda}s}\right) + \frac{R^2}{3D}k_s\sinh\left(\sqrt{\frac{\lambda}{1+\lambda}s}\right)\right]}\right] \tag{23}$$

where s is Laplace variable and tilde denotes a Laplace transformed variable. Next, consider the total mass balance within the entire chamber (gas phase + zeolite)

$$sn_e(\tilde{p} - \tilde{v}) + s\{NC_e\int_0^V \tilde{C}\,dV\} = 0 \tag{24}$$

After substitution of eq 23 into eq 24, a numerical solution of frequency response can be obtained as

dx.doi.org/10.1021/jp507212b | J. Phys. Chem. C 2014, 118, 22166−22180

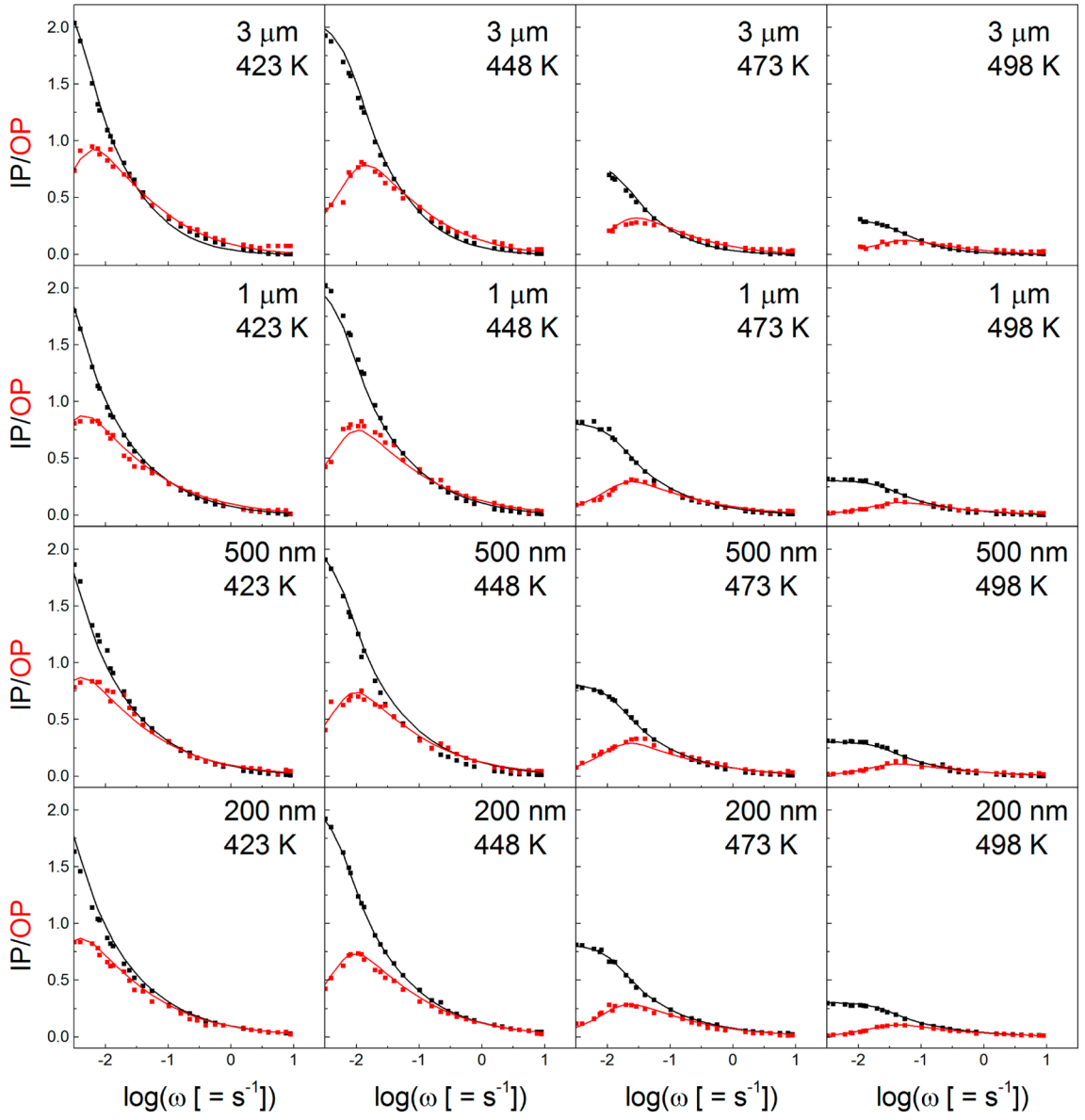

Figure 5. In-phase (IP) and out-of-phase (OP) frequency response of cyclohexane in silicalite-1 with T-Q model fit. Transformed pressure response data represented as in-phase (black) and out-of-phase (red) data collected at each frequency. Solid lines represent the Teixeira–Qi model fit for each temperature.

$$Q = \frac{K(k_s)\frac{R^2}{D}\left\{\sqrt{\frac{1+\lambda}{\lambda s}}\cosh\left(\sqrt{\frac{\lambda}{1+\lambda}}s\right) - \frac{1+\lambda}{\lambda s}\sinh\left(\sqrt{\frac{\lambda}{1+\lambda}}s\right)\right\}}{\left[-\sinh\left(\sqrt{\frac{\lambda}{1+\lambda}}s\right) + \sqrt{\frac{\lambda}{1+\lambda}}s\cosh\left(\sqrt{\frac{\lambda}{1+\lambda}}s\right) + \frac{R^2}{3D}k_s\sinh\left(\sqrt{\frac{\lambda}{1+\lambda}}s\right)\right]} = \frac{\tilde{v}}{\tilde{p}} - 1 \quad (25)$$

Similar to Yasuda's model, eq 25 can be expressed in terms of a real part (in-phase) and imaginary part (out-of-phase). The solution was solved numerically in Matlab and expressed as

$$\frac{v}{p}\sin\phi = \mathrm{Re}(Q) \quad (26)$$

$$\frac{v}{p}\cos\phi - 1 = -\mathrm{Im}(Q) \quad (27)$$

Data fitting was performed using Matlab by performing a four-parameter least-squares optimization for parameters D, K, k_s, and k_{-s}. The optimization was performed simultaneously for all particle sizes at each temperature to minimize the square of the summed errors of the in-phase and out-of-phase frequency response data and model fits.

4.0. RESULTS

Pressure–volume response curves were obtained for the five particles described in Table 2 at four temperatures in the range of 423–513 K. Periodic, steady-state data were obtained for each particle size at frequencies ranging between 0.0025 and 10 Hz and were transformed to the in-phase and out-phase functions described by the left side of eqs 6 and 7, respectively (Figure 5, data points).

The base case (Figure 4, model I) was first used to fit the experimental data. However, the base model poorly fit the data in small particles because of the cross of the in-phase and out-of-phase data. As is noted in the literature, poor fitting is indicative of a "surface barrier" or "surface resistance" near the zeolite

dx.doi.org/10.1021/jp507212b | J. Phys. Chem. C 2014, 118, 22166–22180

Table 3. Proposed Mechanisms of Surface Barriers and Associated Kinetic Criteria

mechanism/limitation	ref	criteria met	criteria not met	conclusion
internal barriers				
Subcrystal grain boundaries, intergrowths and internal defects slow intracrystalline transport.	12, 19, 51, 52	$D_{app} < D$ E_{app} = constant	$D \neq f(R)$	Does not account for size dependence.
adsorption−desorption (Yasuda surface resistance)				
Time scale associated with adsorption−desorption to the outer surface from the gas phase is slow relative to internal diffusion.	21, 28, 44	$\tau_{app} = f(R) = \frac{R^2}{D} + \frac{1}{k_a P} + \frac{1}{k_d}$ $k_a \neq f(R)$ $k_d \neq f(R)$	$D \neq f(R)$ $k_a P \ll 10^{13}\ s^{-1}$	Does account for size dependence. Surface parameters do not scale properly.
pore narrowing				
Surface pores are narrowed or partially obstructed causing an energetic barrier to penetrate the surface.	12, 56, 57	$\tau_{app} = f(R) = \frac{R^2}{D} + \frac{1}{k_a P} + \frac{1}{k_d}$	$k_s \neq k_{-s}$ $E_{a,-s} > E_a$	Does account for size dependence.Surface kinetics are not symmetrical. Increase to energetic barrier is not observed.
pore blockage				
A substantial fraction of pores are blocked at the surface, causing an increase in the diffusional length scale associated with release.	12, 45, 62, 63	$\tau_{app} = f(R) = \frac{R^2}{D} + \frac{1}{k_a P} + \frac{1}{k_d}$ $k_s \neq k_{-s}$ $E_a = E_{-s} > E_s$	−	Does account for size dependence and asymmetric surface barriers with energetics described by intracrystalline diffusion barriers and adsorption enthalpies.

surface, and a model accounting for surface limitations is required to accurately describe the mass transfer process.[28]

Model parameter optimizations for Yasuda's surface resistance model (eqs 9−12, model II) and the T-Q surface resistance model (eqs 25−27, model IV) were performed using a log-normal least-squares optimization for the respective in-phase and out-of-phase functions, as shown in Figure S1 of the Supporting Information and Figure 5, respectively. The Yasuda surface resistance model requires a three- parameter fit (D, κ_a, K) to determine the intracrystalline diffusion constant, Langmuir rate constant, and the equilibrium constant between surface adsorbed species and bulk gas phase species. In the case of the T-Q model, the surface limitation is captured by the two parameters, k_s and k_{-s}, which represent the forward and reverse mass transfer rates at the zeolite surface, respectively. In both cases, characteristic mass transfer time scales are observed as the corner frequencies of the out-of-phase function, represented by the peaks in the data of Figure 5. As temperature increases, peaks are observed to shift to higher frequencies (right), indicating faster overall transport rates. Similarly, as particle sizes decreases, a corresponding shift is observed to higher frequencies, again indicating a transition to faster transport rates as is typical for diffusion-controlled processes. Data for the large particles are characteristic of intracrystalline diffusion-controlled systems, where the in-phase and out-of-phase data do not cross; the single corner frequency occurs at a frequency characteristic of the diffusional time constant. Also, for large particles, the base model fit (model I) exhibits fitting parameters similar to those obtained by the Yasuda surface resistance model (model II). For small particles, however, the overlap between the two characteristic functions becomes significant, indicating an increasing transition to surface-controlled mass transfer limitations.

By introducing a rate limitation at the surface, both the Yasuda surface resistance and T-Q models fit the raw experimental data well, as observed in Figure 5 and Figure S1 of the Supporting Information. Fitting parameters for the Yasuda surface resistance and T-Q model are summarized in Table 3. For both model fits, the equilibrium constant obtained from fitting (K) is associated with Henry's constant by eq 8. The equilibrium constant was activated in accordance with the van't Hoff relationship[43]

$$K = K_0 \exp\left(\frac{-\Delta U_0}{RT}\right) = K_0 \exp\left(\frac{-\Delta H_s^{ads}}{RT} - 1\right) \quad (28)$$

where ΔH_s^{ads} is the heat of adsorption associated with cyclohexane reversibly adsorbing or desorbing from the *outer zeolite surface*. The heat of adsorption to the *outer surface* of the zeolite is shown here to be ΔH_s^{ads} = 45.8 ± 11.4 kJ/mol. As expected, this parameter is independent of particle size and is a function of only temperature and the equilibrium pressure.

For model II (Yasuda surface resistance), the apparent diffusivity (D_{app}) is a strong function of particle size, as shown in Figure 3. The data exhibit an Arrhenius relationship for diffusion for each particle with constant activation energy. However, the pre-exponential is observed to decrease drastically with decreasing particle size, indicating that a second, size-dependent phenomenon becomes rate relevant in small particles. Dependence of the apparent diffusion coefficient with particle size is explored in greater detail in the section 5.0.

The T-Q model accounts for both gas−surface equilibrium and surface resistance, and the transport time scales for intracrystalline diffusion are extracted and plotted versus inverse temperature. Measured values of diffusivity collapse for all zeolite particles, indicating intracrystalline diffusion is independent of particle size, as is physically expected. Both constants describing the rate through the surface (k_s and k_{-s}) and apparent diffusivity are temperature-activated in accordance with an Arrhenius relationship, as shown below.

$$D = D_0 \exp\left(-\frac{E_a}{RT}\right)$$
$$k_s = k_{s,0} \exp\left(-\frac{E_{a,s}}{RT}\right)$$
$$k_{-s} = k_{-s,0} \exp\left(-\frac{E_{a,-s}}{RT}\right) \quad (29)$$

where E_a, $E_{a,s}$, and $E_{a,-s}$ are the activation energies for diffusion, uptake, and release from the exterior/interior surface, respectively. If all silicalite-1 particles are assumed to share the same surface and bulk structures, all respective activation

dx.doi.org/10.1021/jp507212b | J. Phys. Chem. C 2014, 118, 22166−22180

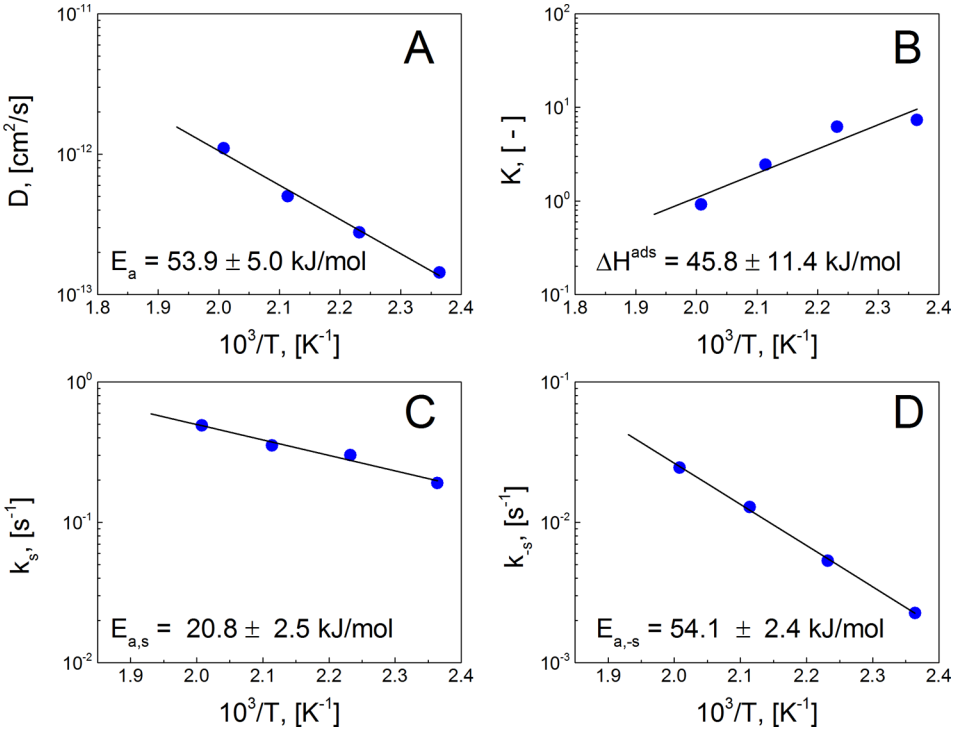

Figure 6. Teixeira−Qi zeolite mass transfer model parameters. The four-parameter Teixeira−Qi model was fit at each temperature, with respective constants plotted with inverse temperature. All parameters are temperature-activated, with the activation energies of the intracrystalline diffusivity and surface release matching.

energies should be constant irrespective of particle size, which is consistent with the model fits presented here and in good agreement with literature values for diffusion of cyclohexane in silicalite-1.[4]

5.0. DISCUSSION

Three models were independently evaluated to describe the volume−pressure frequency response data for cyclohexane in silicalite-1. The base case (model I), has been widely used to describe diffusion-controlled mass transport in microporous materials. This model arises from solving the one-dimensional spherical transient diffusion system with a sinusoidal boundary condition describing the equilibrated surface concentration (Henry's Law). As equilibrium is always assumed at the surface in this model, the externally observed pressure response is dependent on the equilibrium constant, diffusivity, and particle size only. The base model works well to describe systems in which diffusion within the bulk of the crystal is rate-dominating and all other rate limitations (adsorption−desorption, external boundary layers, surface defects, internal grain boundaries, etc.) are negligible. These criteria often hold true for slow-diffusing molecules and for large particles ($D/R^2 < 10^{-3}$ s^{-1}). Experimentally, deviation from the base case is directly observed by a cross in the in-phase and out-of-phase function and data. In the work presented in this study, as with other cases in the literature,[28,44] the base case was not able to describe the cyclohexane−silicalite-1 system for small particles. For this reason, other models were considered that describe series transport processes.

In the case of a surface limitation, macroscopic transport observed experimentally is described by two series processes: Fickian diffusion in the micropores and transport at or through the surface. In the case in which the time scale for the surface transport is sufficiently small ($\tau_s \ll \tau_D$), surface transport is not rate-limiting and experimentally characterized mass transfer collapses to the base case. However, if there exists a transport limitation at the surface with a time scale on the order of or higher than the diffusional time scale, then the limitation must be mathematically described to fit the experimental data. The frequency response model for the base case can then be modified replacing the assumption of equilibrium at the particle surface in lieu of a kinetic boundary condition.

The mostly widely used model to describe frequency response mass transfer data containing surface limitations, or "surface barriers", is described by Yasuda.[44] In this model, the kinetic rate limitation through the surface is assumed to arise from the rate of adsorption−desorption. Langmuirian kinetics (eq 1) are assumed to describe the competitive rates of adsorption and desorption, resulting in a modified boundary condition and solution to the in-phase and out-of-phase curves. Unlike the base model, the Yasuda model was able to fit the experimental response curves (Figure S1 in the Supporting Information) by introducing the additional fitting parameter κ_{-A}. The in-phase and out-of-phase data can then be fit by $f(D, K, \kappa_{-A})$ where the three parameters represent the bulk diffusivity, the equilibrium constant (ratio of adsorption−desorption rate constants), and lumped Langmuir parameter (function of the adsorption−desorption constants). Alternatively, this can be evaluated in terms of more familiar parameters such that the data can be fit as $f(D, k_a, k_d)$, where the response is now a function of the Langmuir rate parameters for adsorption and desorption described by eq 1. The fitting parameters extracted from Figure S1 in the Supporting Information are represented in Table 2. Whereas the introduction of a rate limitation at the surface was able to fit the raw data obtained from frequency response, the extracted parameters do not accurately describe the physical system; the diffusion coefficients demonstrate strong particle size depend-

dx.doi.org/10.1021/jp507212b | J. Phys. Chem. C 2014, 118, 22166−22180

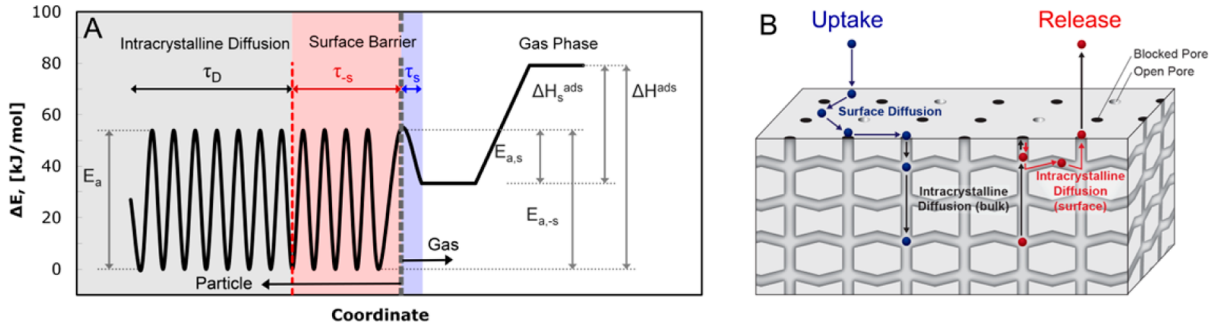

Figure 7. Zeolite mass transport with surface pore blockages. (A) Energy diagram for intracrystalline bulk diffusion (E_a, τ_D), surface heat of adsorption (ΔH_s^{ads}), uptake surface barrier ($E_{a,s}$, τ_s), release surface barrier ($E_{a,-s}$, τ_{-S}), and heat of adsorption (ΔH^{ads}). (B) During uptake (blue), surface pore blockages cause a molecule to adsorb and undergo surface diffusion until finally locating and entering into an open pore. During the release from the zeolite (red), a molecule diffuses to the surface after which it must continue to diffuse within the lattice until locating and exiting an open pore.

ence, which is inconsistent with Fick's law for configurational diffusion through microporous channels. Identical molecule–pore combinations should exhibit identical bulk diffusion coefficients regardless of particle size.

The Teixeira–Qi model was developed to introduce an asymmetric surface barrier that removes the constraint relating the adsorption and desorption rate constants to a Langmuir relationship ($K_{eq} = k_a/k_d$). Similar to the previous case, this model utilizes a boundary condition arising from the balance of the diffusive flux and the flux through the surface. While equilibrium is still assumed between the gas phase and the external surface (similar to the base and Yasuda surface resistance cases), the kinetic steps of permeating into and out of the surface independently contribute to the overall transport time scales. As shown in Figure 5, the T-Q model fit to the raw frequency response data is similar to that of the Yasuda surface resistance model described earlier. The crossing of the in-phase and out-of-phase curves is well-captured, and the fitting parameters are summarized in Figure 6 and Table 2. However, a single set of temperature-activated fitting parameters is able to accurately describe cyclohexane transport in all particles across multiple orders of magnitude in size. The diffusivity parameter collapses onto a single curve which obeys the Arrhenius relationship for diffusion (eq 29). The additional two parameters represent the rate constants for penetrating into and out of the surface (k_s, k_{-s}), each of which is temperature-activated in a similar manner (eq 29). The rate entering into the pores was observed to be up to an order of magnitude higher than that observed describing the release from the pores, which is consistent with interference microscopy studies performed during both uptake and desorption of large particles, in which the transport through the surface was observed to be an order of magnitude faster during uptake.[45]

5.1. Temperature Activation. Literature-reported values for diffusion of cyclohexane in silicalite-1 often report similar activation energies (30–60 kJ/mol),[4,12,14,46–49] despite orders of magnitude differences in diffusivity. The activated step in all these cases is claimed to be intracrystalline diffusion of cyclohexane within microporous MFI channels. Figure 7 depicts the energies associated with the series processes of intracrystalline diffusion, transport through the surface and adsorption–desorption to the gas phase. The two surface parameters exhibited different activation energies, indicating the asymmetric nature of the surface barrier. The parameter for uptake into the surface exhibited an activation energy of $E_{a,s} = 20.8 \pm 2.5$ kJ/mol, whereas exiting the surface was activated similar to that of diffusion, $E_{a,-s} = 54.1 \pm 2.4$ kJ/mol. In this work, an intracrystalline activation energy of 53.9 ± 5.0 kJ/mol was observed, which is consistent with previously reported values. The equilibrium constant was also activated in accordance with the van't Hoff relationship (eq 28). In this study, the heat of adsorption *to the surface* (ΔH_s^{ads}) was observed as 45.8 ± 11.4 kJ/mol.

Kinetics of cyclohexane transport from inside the particle to the gas phase are thermodynamically consistent with the heat of adsorption of cyclohexane. As shown in Figure 7, the heat of adsorption of cyclohexane in silicalite-1 should be related to the surface release activation energy ($E_{a,-s}$), surface uptake activation energy ($E_{a,s}$), and the heat of adsorption to the surface (ΔH_s^{ads}) by the following relationship

$$\Delta H^{ads} = E_{a,-s} - E_{a,s} + \Delta H_s^{ads}$$

$$\Delta H^{ads}(\text{kJ/mol}) = (54.1 \pm 2.4) - (20.8 \pm 2.5) + (45.8 \pm 11.4)$$

$$= 79.1 \pm 16.3 \text{ kJ/mol} \quad (30)$$

The sum of the three energy barriers when added by eq 30 equals 79.1 ± 16.3 kJ/mol, which is inclusive of values of the heat of adsorption of cyclohexane in silicalite-1 when accounting for experimental error. Previous studies have measured the heat of adsorption into large silicalite-1 particles to be 63.2 kJ/mol[43] and 70 kJ/mol.[50] Close agreement by eq 30 between measured kinetics and independently measured heat of adsorption provides strong support for the validity of the T-Q model.

5.2. Transport Barriers. Barriers to intracrystalline diffusion have been proposed in numerous forms ranging from the intergrowths, internal grain boundaries, and pore saturation to kinetically limited adsorption–desorption, surface pore narrowing, and surface pore blockages. Surface barriers and their potential applications to the microporous materials examined in this study are explored here and summarized in Table 3.

5.2.1. Internal Barriers. Intrinsic internal barriers are proposed to exist resulting from particle synthesis during crystal growth of MFI-structured zeolites.[51,52] Silicalite-1 is not a single crystal but rather is composed of several subcrystals whose interface presents an internal grain boundary with pore misalignments as small as 0.5–2°.[19] Additionally, both intergrowths and internal defects are possible within single particles. While such internal barriers are present and likely contribute to the macroscopically observed rate, they are not thought to lead to the drastic size-dependent inhibition observed in these experiments and others.[12]

dx.doi.org/10.1021/jp507212b | J. Phys. Chem. C 2014, 118, 22166–22180

5.2.2. Surface Barriers: Energetic. An activation barrier exists for a molecule being transported from a bulk gas to the inner surface of a zeolite prior to entering the purely intracrystalline transport domain. During uptake, a molecule travels in the gas phase to the particle, adsorbs to the outer surface, reorients, and enters into a pore. Though usually considered fast (surface permeability $\sim 10^{-5}-10^{-7}$ cm/s)[45] when compared to configurational diffusion ($<10^{-6}$ cm^2/s),[53] it can present a possible rate limitation for small particles. As concentrations are dilute, no substantial boundary layer is expected, making the first possible rate limitation associated with the adsorption and desorption of a molecule from the gas phase in close proximity to the outer solid surface. For zeolite systems, this rate is captured by the Langmuir relationship, where $\tau_s = 1/(k_a P)+1/k_d$. In the case of this study, typical values of this time constant range from 10^0 to 10^2 s, which is shorter than the smallest diffusional time ($\tau_D > 10^2$ s), again validating the assumption of equilibrium between the surface and the gas phase.

The final step is associated with both enthalpic and entropic molecular confinement at or near the pore surface. The enthalpic contribution to the rate of pore entering is associated with the guest molecule (cyclohexane; critical diameter, 6.0−6.9 Å; kinetic diameter, 5.7 Å)[43] undergoing a high-energy transition to enter within the micropores of silicalite-1 (~5.5 Å).[54]

The entropic contribution of molecules entering pores, which is thought to apply during uptake, can potentially lead to a decrease in the pre-exponential for diffusion as described by Ford et al.[55] and the relationship[21]

$$D_0 = \frac{a^2 w(T)}{2\pi} \exp\left(-\frac{\Delta S(T)}{k_B}\right) \tag{31}$$

Molecular rearrangement is expected to reduce the pre-exponential for diffusion during the uptake process, as no such rearrangement is needed upon release. Additionally, the temperature contribution to the diffusion coefficient from the pre-exponential is not dominant when compared to the enthalpic effect ($\exp(-E_a/(RT))$); therefore, the observed temperature dependence should remain attributed to intracrystalline diffusion. In this work, it is shown that the activation energy to enter the pores ($E_{a,s}$ = 20.8 kJ/mol) is substantially less than that of intracrystalline diffusivity (E_a = 53.9 kJ/mol), indicating that the mechanism for pore blockage during uptake is likely not due to molecular rearrangement.

Enthalpic barriers during uptake are possible in the case of surface pore narrowing (i.e., structural changes to pores at the surface).[56,57] In this case, deviation from the MFI structure at the surface could result in a higher energy barrier through a surface defect ($E_{a,s} > E_a$). However, previous experimental work studying the desorption process (ZLC) has demonstrated that no significant difference in activation energies was observed between particles exhibiting surface barrier transport control (small particles) and those exhibiting purely intracrystalline diffusion control (large particles).[12] This result is again affirmed here, where the activation energy for the intracrystalline diffusivity is comparable to the rate constant describing release from the surface (E_{-s} = 54.1 kJ/mol ~ E_a = 53.9 kJ/mol) and less than that into the surface (E_s = 20.8 kJ/mol < E_a = 53.9 kJ/mol). For these reasons, it is concluded that the elementary step governing release of molecules from the intracrystalline domain to the bulk gas *at the surface* is likely similar to the mechanism of mass transfer by intracrystalline diffusion (and different from the mechanism describing entering *into the surface*).

5.2.3. Surface Barriers: Structural. Simply put, surface pore blockages can be present when surface defects block the entrance to micropores such that diffusing guest molecules cannot enter or exit. In this case, the flux into a surface is controlled by adsorption, surface diffusion to an open pore, and entering into the pore. Flux out of a particle through a surface is controlled by intracrystalline diffusion until a molecule reaches an open pore at the surface. The former is observed to be rate-controlling in guest uptake, while the latter is observed during release. By using the frequency response technique with the T-Q model, the two processes are decoupled at the surface and the kinetic constants and activation energies are determined. As depicted in Figure 7, molecules diffusing out of the pores encounter an additional diffusional path length (δ) which presents as a slower macroscopically observed transport rate ($\tau = R^2/D + \delta^2/D$). The additional length does not, however, affect the activation energy because the mechanism of transport remains the same. In the uptake case, the observed transport time scale is associated with a molecule adsorbing to the external surface, diffusing to an open pore, and entering the pore.

The exact nature or structural contribution of surface pore blockages is difficult to elucidate experimentally. This challenge arises from an inability to fully characterize surface termination of the crystalline structure which results from crystal growth. The manifestation of surface blockages could arise from several types of structural defects. First, large areas of uncoordinated lattice or amorphous silica may exist in patches on the surface such that entire regions are blocked, causing patches of surface barriers. Alternatively, pore blockages could be distributed across the particle surface by surface-terminated configurations that block pores or obstruct molecules from exiting a pore at the surface.

The presence of surface defects resulting from amorphous or unaligned islands on the surface has been discussed in literature in varying contexts (defects, terraces, islands, nanoparticle aggregation, growth mechanism).[35,58−62] Such defects are shown to arise in some cases from interpenetrating dangling silanol bonds causing terraces at the surface.[35] However, these features constitute a relatively small fraction of total surface pores, and pore blockages across a wider area must be considered.[63]

The work of Kärger and co-workers has described the presence of physical surface pore blockages as a possible mechanism for describing this surface resistance to diffusion in microporous materials.[23,45,63−65] In MFI, it was proposed that most of the surface pores exhibit blockages, with only a very small fraction allowing transport through the surface.[45] Such blockages are proposed to be surface structure dependent; thus, the fraction of blocked pores is expected to remain constant irrespective of particle size. Furthermore, a comparison of transport rates across "cracks" in the bulk portion of a zeolite (fully open pores) versus the outer surface pores reveals slower transport across the as-synthesized surface.[58] Surface etching has been shown to have no effect on these more prominent barriers.[58]

The observed hindered surface permeability is consistent with the theory that pore blockages arise from random surface terminations and amorphous blockages, where the outermost pores differ structurally from the bulk.[66] With current imaging techniques, however, surface terminations are difficult to visualize experimentally, and the presence of subnanometer defects at the surface is not commonly characterized. Experimental techniques including atomic force microscopy (AFM),[35,59,67] scanning electron microscopy (SEM),[60] and high-resolution transmission electron microscopy (HRTEM)[59,67,68]

dx.doi.org/10.1021/jp507212b | J. Phys. Chem. C 2014, 118, 22166−22180

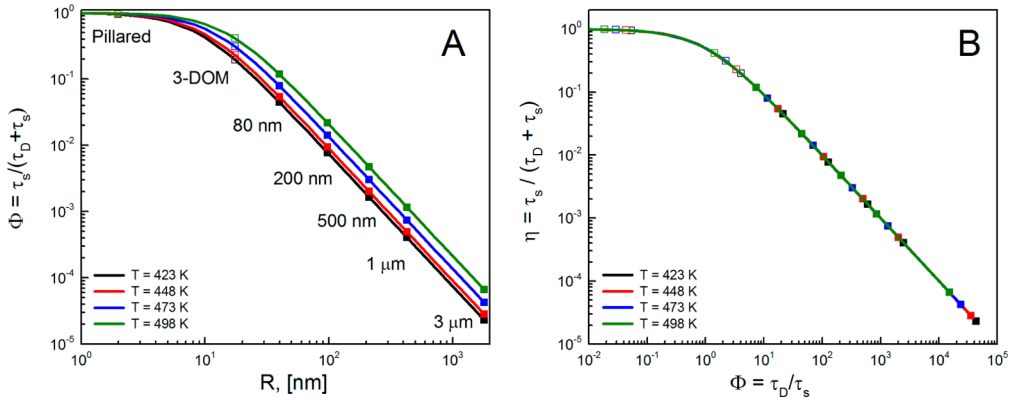

Figure 8. Surface and bulk mass transfer time constants for mesoporous materials. Experimentally measured time constants allow for determination of relative surface barriers (closed symbols) in silicalite-1. Surface limitations in microporous materials are shown to be rate relevant in small particles, and calculations for hierarchical materials (open symbols) including the 3DOm-i and Pillared materials are predicted to experience transport rates dominated by surface barriers.

have been used to resolve the postsynthesis surface structure of zeolites, with the best resolution being on the order of several angstroms. While large facets including crystal faces, steps, islands, and grain boundaries are observed on the order of nanometers, surface termination, pore openings, and small defects leading to blockage are considerably more difficult to capture. Existing experimental techniques are unable to definitively describe surface termination and pore blockages on the surface of zeolites.[69] This level of description requires resolution of 1 Å or less to observe the small pore size of the 10-member MFI rings (5.6 Å). Additionally, it has also been proposed that the use of TEM and STEM to examine the surface of crystals for pore blockage or restrictions will provide an artificially clean appearing surface because of the ability of the technique to penetrate the surface.[60]

Theoretical studies have attempted to describe the growth and surface termination of zeolites. The structure of the pores at the surface is believed to be a direct result of the final growth termination steps during particle synthesis. Recent work by Lupelescu and Rimer has utilized *in situ* AFM to examine the layered growth mechanism and confirm the initial deposition of silica nanoparticles followed by directed rearrangement of the amorphous silica to the MFI structure.[61] The resulting surface represents a thermodynamically stable termination of the dangling Si−O bonds. The pores at the surface are modeled computationally using free energy surface minimization techniques, allowing for the prediction of surface termination structures.[70,71] In MFI, FTIR microscopy on the surface of silicalite-1 has been used to explore the defect density and determine that locally spaced silanol groups are likely hydrogen bonded.[35] This bridging across so-called "defects" may lead to pore blockages. At this point, a significant gap exists in the literature with respect to both direct experimental visualization and indirect theoretical calculations of surface pore blockages in zeolites.

5.3. Implications for Hierarchical Materials. Moving forward, surface barriers will have profound impact on the use of zeolites in hierarchical materials in which the diffusional length scales are drastically decreased with the introduction of mesopores. In such materials, groups are able to synthesize microporous materials with length scales on the order of a single lattice cell (~2 nm, MFI).[4,11] While from a practical standpoint these materials are observed to exhibit substantially improved mass transport properties when compared to those of traditional large particle zeolites, significant limitations have been shown to still exist.[4] By extracting the measured time constants for the series transport steps described in this work, a relationship is constructed relating the time scale associated with penetrating the surface barrier to that of the bulk particle. Figure 8 shows the experimental values for the cyclohexane−silicalite-1 system at several temperatures and particle sizes. As particle size decreases, a linear relationship is observed versus particle size, as expected by an intracrystalline diffusion-controlled system where the time constant scales with the square of particle size. Plotted at smaller particle sizes, however, are calculated time constants for the hierarchical particles (3DOm-i and SPP). These materials tend toward a purely surface-controlled case which has been shown to be rate-dominating in these small particles. While the establishment of the asymmetric structural surface barrier described in this work moves toward understanding the transport limitations at the surface of zeolites, further understanding is needed to elucidate the cause and means of removal of such barriers, thus allowing mesoporous materials to achieve their full potential.

6.0. CONCLUSIONS

For the first time, surface barriers in silicalite-1 are characterized experimentally to exhibit asymmetric kinetic and energy dependences, whereby separate mechanisms are rate-controlling for entering and exiting surface pores. Using the frequency response technique, surface barriers are shown to become rate relevant and eventually dominate mass transport into and out of small silicalite-1 particles (<100 nm). Mechanistic insight is provided showing the uptake step exhibits a low activation barrier, whereas both intracrystalline diffusion and surface release steps exhibit the same activation energies. Structural blockages at the surface of most pores are proposed to describe the observed surface limitation. Despite kinetic characterization of surface limitations, conclusive evidence of surface pore blockages has yet to resolve the surface of MFI to determine the distribution of surface termination structures to quantify the extent of structural pore blockages.

■ ASSOCIATED CONTENT

Supporting Information

Yasuda surface resistance model fit, raw frequency response data for five particles at all temperatures, and mathematical derivations of the Yasuda base frequency response model as

dx.doi.org/10.1021/jp507212b | J. Phys. Chem. C 2014, 118, 22166−22180

well as the Teixeira−Qi frequency response model. This material is available free of charge via the Internet at http://pubs.acs.org.

AUTHOR INFORMATION

Corresponding Author

*E-mail: hauer@umn.edu.

Author Contributions

§A.R.T. and X.Q. contributed equally.

Notes

The authors declare no competing financial interest.

ACKNOWLEDGMENTS

Financial support was provided by the Catalysis Center for Energy Innovation, a U.S. Department of Energy−Energy Frontiers Research Center (www.efrc.udel.edu) under Award DE-SC0001004. The authors acknowledge Professor Scott Auerbach for valuable insight into adsorption and diffusion in zeolites.

NOMENCLATURE

A = Outer surface concentration
B = Inner surface concentration
C = Concentration within zeolite particle
C_e = Concentration at equilibrium
$\bar{c}$ = Dimensionless concentration
$\tilde{C}$ = Laplace transform of dimensionless concentration
D = Diffusivity
E = Activation energies
$\underset{\sim}{f}$ = Defined as $f \equiv \bar{c}\eta$
$\tilde{f}$ = Laplace transform of f
G = Transfer function $\equiv \tilde{p}/\tilde{v}$
J_s = Surface flux
J_D = Diffusion flux
k_s = Uptake mass transfer coefficient
k_{-s} = Release mass transfer coefficient
K_H = Henry's constant
K = Defined as $K = (RTV_s/V_e)K_H$ in the base case and $K = NV_sC_e/n_e$ in the T-Q model
N = Number of zeolite particles
P = Pressure of the system
P_e = Pressure at Equilibrium
$\tilde{P}$ = Laplace transform of pressure
$\bar{p}$ = Dimensionless pressure
$p(t)$ = Pressure amplitude ratio
Q = Defined as $Q = \bar{v}/\bar{p} - 1$
s = Laplace variable
V_s = Volume of zeolite particle
V = Volume of the system
V_e = Volume at equilibrium
v = Volume amplitude ratio
$\tilde{v}$ = Laplace transform of volume
X' = Amount of species in gas phase
X = Amount of species in solid phase
η = Dimensionless length = r/R
η' = Defined as $\sqrt{(2\ \omega\ R^2/D)}$
η^* = Defined as $\eta^* = (\omega^*/2)^{1/2}$
λ = Dimensionless number = t_D/t_s
τ = Dimensionless time scale
ϕ = Phase lag
ω = Angular frequency
ω^* = Reduced angular frequency

REFERENCES

(1) Auerbach, S. M.; Carrado, K. A.; Dutta, P. K. *Handbook of Zeolite Science and Technology*; M. Dekker: New York, 2003.

(2) van den Bergh, J.; Gascon, J.; Kapteijn, F. Diffusion in Zeolites − Impact on Catalysis. In *Zeolites and Catalysis*; Wiley-VCH Verlag GmbH & Co. KGaA: Weinheim, Germany, 2010; pp 361−387.

(3) Fan, W.; Snyder, M. A.; Kumar, S.; Lee, P.-S.; Yoo, W. C.; McCormick, A. V.; Lee Penn, R.; Stein, A.; Tsapatsis, M. Hierarchical Nanofabrication of Microporous Crystals with Ordered Mesoporosity. *Nat. Mater.* **2008**, *7*, 984−991.

(4) Chang, C.-C.; Teixeira, A. R.; Li, C.; Dauenhauer, P. J.; Fan, W. Enhanced Molecular Transport in Hierarchical Silicalite-1. *Langmuir* **2013**, *29*, 13943−13950.

(5) Zhang, X. Y.; Liu, D. X.; Xu, D. D.; Asahina, S.; Cychosz, K. A.; Agrawal, K. V.; Al Wahedi, Y.; Bhan, A.; Al Hashimi, S.; et al. Synthesis of Self-Pillared Zeolite Nanosheets by Repetitive Branching. *Science* **2012**, *336*, 1684−1687.

(6) Zhang, X. Y.; Liu, D. X.; Xu, D. D.; Asahina, S.; Cychosz, K. A.; Agrawal, K. V.; Al Wahedi, Y.; Bhan, A.; Al Hashimi, S.Direct Synthesis of Self-Pillared Zeolite Nanosheets by Repetitive Branching. *Abstracts of Papers*, 244th National Meeting of the American Chemical Society, Philadelphia, PA, Aug 19−23, 2012244

(7) Choi, M.; Na, K.; Kim, J.; Sakamoto, Y.; Terasaki, O.; Ryoo, R. Stable Single-Unit-Cell Nanosheets of Zeolite MFI as Active and Long-Lived Catalysts. *Nature (London, U.K.)* **2009**, *461*, 246−249.

(8) Gao, P.; Tai, M. H.; Sun, D. D. Hierarchical TiO_2/V_2O_5Multifunctional Membrane for Water Purification. *ChemPlusChem* **2013**, *78*, 1475−1482.

(9) Du, K.; Liu, Y. Y.; Wathuthanthri, I.; Choi, C. H. Fabrication of Hierarchical Nanostructures Using Free-Standing Trilayer Membrane. *J. Vac. Sci. Technol., B: Microelectron. Nanometer Struct.—Process., Meas., Phenom.* **2013**, *31*, 06FF04−06FF041-11.

(10) Yacou, C.; Ayral, A.; Giroir-Fendler, A.; Baylet, A.; Julbe, A. Catalytic Membrane Materials with a Hierarchical Porosity and Their Performance in Total Oxidation of Propene. *Catal. Today* **2010**, *156*, 216−222.

(11) Zhang, X.; Liu, D.; Xu, D.; Asahina, S.; Cychosz, K. A.; Agrawal, K. V.; Al Wahedi, Y.; Bhan, A.; Al Hashimi, S.; et al. Synthesis of Self-Pillared Zeolite Nanosheets by Repetitive Branching. *Science* **2012**, *336*, 1684−1687.

(12) Teixeira, A. R.; Chang, C.-C.; Coogan, T.; Kendall, R.; Fan, W.; Dauenhauer, P. J. Dominance of Surface Barriers in Molecular Transport through Silicalite-1. *J. Phys. Chem. C* **2013**, *117*, 25545−25555.

(13) Bonilla, M. R.; Valiullin, R.; Kärger, J.; Bhatia, S. K. Understanding Adsorption and Transport of Light Gases in Hierarchical Materials Using Molecular Simulation and Effective Medium Theory. *J. Phys. Chem. C* **2014**, *118*, 14355−14370.

(14) Cavalcante, C. L., Jr.; Ruthven, D. M. Adsorption of Branched and Cyclic Paraffins in Silicalite. 2. Kinetics. *Ind. Eng. Chem. Res.* **1995**, *34*, 185−191.

(15) Ruthven, D. Diffusion in Zeolites—A Continuing Saga. *Adsorption* **2010**, *16*, 511−514.

(16) Kärger, J. Measurement of Diffusion in Zeolites—A Never Ending Challenge? *Adsorption* **2003**, *9*, 29−35.

(17) Kortunov, P.; Vasenkov, S.; Chmelik, C.; Karger, J.; Ruthven, D. M.; Wloch, J. Influence of Defects on the External Crystal Surface on Molecular Uptake into MFI-Type Zeolites. *Chem. Mater.* **2004**, *16*, 3552−3558.

(18) Newsome, D. A.; Sholl, D. S. Molecular Dynamics Simulations of Mass Transfer Resistance in Grain Boundaries of Twinned Zeolite Membranes. *J. Phys. Chem. B* **2006**, *110*, 22681−22689.

(19) Karwacki, L.; Kox, M. H. F.; Matthijs de Winter, D. A.; Drury, M. R.; Meeldijk, J. D.; Stavitski, E.; Schmidt, W.; Mertens, M.; Cubillas, P.; et al. Morphology-Dependent Zeolite Intergrowth Structures Leading to Distinct Internal and Outer-Surface Molecular Diffusion Barriers. *Nat. Mater.* **2009**, *8*, 959−965.

(20) Ruthven, D. M. Transport in Microporous Solids: An Historical Perspective. In *Fluid Transport in Nanoporous Materials*; Conner, W. C.,

Fraissard, J., Eds.; Springer: Dordrecht, The Netherlands, 2006; Vol. *219*; pp 9−40.
(21) Kärger, J.; Vasenkov, S.; Auerbach, S. M. *Diffusion in Zeolites*; Auerbach, S. M., Ed.; Marcel Dekker Inc.: New York, 2003.
(22) Gupta, A.; Snurr, R. Q. A Study of Pore Blockage in Silicalite Zeolite Using Free Energy Perturbation Calculations. *J. Phys. Chem. B* **2005**, *109*, 1822−1833.
(23) Hibbe, F.; Chmelik, C.; Heinke, L.; Pramanik, S.; Li, J.; Ruthven, D. M.; Tzoulaki, D.; Kärger, J. The Nature of Surface Barriers on Nanoporous Solids Explored by Microimaging of Transient Guest Distributions. *J. Am. Chem. Soc.* **2011**, *133*, 2804−2807.
(24) Ruthven, D.; Brandani, S.; Eic, M. Measurement of Diffusion in Microporous Solids by Macroscopic Methods Adsorption and Diffusion. In *Adsorption and Diffusion*; Karge, H., Weitkamp, J., Eds.; Springer: Berlin/Heidelberg, 2008; Vol. *7*; pp 45−84.
(25) Ruthven, D. M. Transport in Microporous Solids Part II: Measurement of Micropore Diffusivities. In *Fluid Transport in Nanoporous Materials*; Conner, W. C., Fraissard, J., Eds.; Springer: Dordrecht, The Netherlands, 2006; Vol. *219*; pp 151−186.
(26) Ghi, P. Y.; Hill, D. J. T.; Whittaker, A. K. PFG NMR Measurements of the Self-Diffusion Coefficients of Water in Equilibrium Poly(Hema-*co*-Thfma) Hydrogels. *Biomacromolecules* **2002**, *3*, 554−559.
(27) Iliyas, A.; Eic, M.; Zahedi-Niaki, M. H.; Vasenkov, S. Toward Observation of Single-File Diffusion Using the Tracer Zero-Length Column Method. *J. Phys. Chem. B* **2008**, *112*, 3821−3825.
(28) Turner, M. D.; Capron, L.; Laurence, R. L.; Conner, W. C. The Design and Construction of a Frequency Response Apparatus to Investigate Diffusion in Zeolites. *Rev. Sci. Instrum.* **2001**, *72*, 4424−4433.
(29) Gueudré, L.; Bats, N.; Jolimaître, E. Effect of Surface Resistance on Cyclohexane Uptake Curves in Silicalite-1 Crystals. *Microporous Mesoporous Mater.* **2012**, *147*, 310−317.
(30) Ruthven, D. M. Diffusion in Type A Zeolites: New Insights from Old Data. *Microporous Mesoporous Mater.* **2012**, *162*, 69−79.
(31) Karge, H. G.; Karger, J. Application of IR Spectroscopy, IR Microscopy, and Optical Interference Microscopy to Diffusion in Zeolites. In *Adsorption and Diffusion*; Karge, H., Weitkamp, J., Eds.; Springer: Berlin/Heidelberg, 2008; Vol. *7*;135206
(32) Ruthven, D. M. Transport in Microporous Solids - Part II: Measurement of Micropore Diffusivities. *Nato Sci. Ser., II* **2006**, *219*, 151−186.
(33) Yasuda, Y. Frequency Response Method for Study of the Kinetic Behavior of a Gas-Surface System. 1. Theoretical Treatment. *J. Phys. Chem.* **1976**, *80*, 1867−1869.
(34) Watanabe, R.; Yokoi, T.; Tatsumi, T. Synthesis and Application of Colloidal Nanocrystals of the MFI-Type Zeolites. *J. Colloid Interface Sci.* **2011**, *356*, 434−441.
(35) Agger, J. R.; Hanif, N.; Cundy, C. S.; Wade, A. P.; Dennison, S.; Rawlinson, P. A.; Anderson, M. W. Silicalite Crystal Growth Investigated by Atomic Force Microscopy. *J. Am. Chem. Soc.* **2003**, *125*, 830−839.
(36) Yasuda, Y. Frequency-Response Method for Study of Kinetic-Behavior of a Gas−Surface System. 2. An Ethylene-on-Zinc Oxide System. *J. Phys. Chem.* **1976**, *80*, 1867−1869.
(37) Yasuda, Y. Determination of Vapor Diffusion Coefficients in Zeolite by the Frequency Response Method. *J. Phys. Chem.* **1982**, *86*, 1913−1917.
(38) Duncan, W. L.; Möller, K. P. On the Diffusion of Cyclohexane in ZSM-5 Measured by Zero-Length-Column Chromatography. *Ind. Eng. Chem. Res.* **2000**, *39*, 2105−2113.
(39) Langmuir, I. The Adsorption of Gases on Plane Surfaces of Glass, Mica and Platinum. *J. Am. Chem. Soc.* **1918**, *40*, 1361−1403.
(40) Yasuda, Y. Frequency-Response Method for Investigation of Gas-Surface Dynamic Phenomena. *Heterog. Chem. Rev.* **1994**, *1*, 103−124.
(41) Yasuda, Y. Frequency Response Method for Investigation of Various Dynamic Phenomena Occurring Simultaneously in a Gas Zeolite System. *Stud. Surf. Sci. Catal.* **1994**, *84*, 1331−1338.
(42) Ruthven, D.; Brandani, F. ZLC Response for Systems with Surface Resistance Control. *Adsorption* **2005**, *11*, 31−34.
(43) Cavalcante, C. L., Jr.; Ruthven, D. M. Adsorption of Branched and Cyclic Paraffins in Silicalite. 1. Equilibrium. *Ind. Eng. Chem. Res.* **1995**, *34*, 177−184.
(44) Yasuda, Y. Detection of Surface Resistance in a Gas/Porous-Adsorbent System by Frequency Response Method. *Bull. Chem. Soc. Jpn.* **1991**, *64*, 954−961.
(45) Gueudré, L.; Binder, T.; Chmelik, C.; Hibbe, F.; Ruthven, D. M.; Kärger, J. Micro-Imaging by Interference Microscopy: A Case Study of Orientation-Dependent Guest Diffusion in MFI-Type Zeolite Host Crystals. *Materials* **2012**, *5*, 721−740.
(46) Gueudré, L.; Jolimaître, E.; Bats, N.; Dong, W. Diffusion in Zeolites: Is Surface Resistance a Critical Parameter? *Adsorption* **2010**, *16*, 17−27.
(47) Wu, P.; Debebe, A.; Ma, Y. H. Adsorption and Diffusion of C_6 and C_8 Hydrocarbons in Silicalite. *Zeolites* **1983**, *3*, 118−122.
(48) Xiao, J.; Wei, J. Diffusion Mechanism of Hydrocarbons in Zeolites—II. Analysis of Experimental Observations. *Chem. Eng. Sci.* **1992**, *47*, 1143−1159.
(49) Chon, H.; Park, D. H. Diffusion of Cyclohexanes in ZSM-5 Zeolites. *J. Catal.* **1988**, *114*, 1−7.
(50) Magalhães, F. D.; Laurence, R. L.; Conner, W. C. Diffusion of Cyclohexane and Alkylcyclohexanes in Silicalite. *J. Phys. Chem. B* **1998**, *102*, 2317−2324.
(51) Vasenkov, S.; Böhlmann, W.; Galvosas, P.; Geier, O.; Liu, H.; Kärger, J. PFG NMR Study of Diffusion in MFI-Type Zeolites: Evidence of the Existence of Intracrystalline Transport Barriers. *J. Phys. Chem. B* **2001**, *105*, 5922−5927.
(52) Chmelik, C.; Kortunov, P.; Vasenkov, S.; Kärger, J. Internal Transport Resistances and Their Influence on Diffusion in Zeolites as Traced by Microscopic Measuring Techniques. *Adsorption* **2005**, *11*, 455−460.
(53) Ruthven, D. M. Transport in Microporous Solids. In *Fluid Transport in Nanoporous Materials*; Conner, W. C., Fraissard, J. P., Eds.; Springer (in cooperation with NATO Public Diplomacy Division): Dordrecht, The Netherlands, **2006**.
(54) Theodorou, D.; Wei, J. Diffusion and Reaction in Blocked and High Occupancy Zeolite Catalysts. *J. Catal.* **1983**, *83*, 205−224.
(55) Ford, D. M.; Glandt, E. A Molecular Simulation Approach to Studying Mass Transfer Across Surface Barriers. In *Access in Nanoporous Materials*. Pinnavaia, T., Thorpe, M., Eds.; Springer-Verlag: New York, 2002; pp 319−334.
(56) Reitmeier, S. J.; Jentys, A.; Lercher, J. A. Understanding Transport in MFI-Type Zeolites on a Molecular Basis. In *Ideas in Chemistry and Molecular Sciences: Advances in Nanotechnology, Materials and Devices*; Wiley-VCH Verlag GmbH & Co. KGaA: Weinheim, Germany, 2010; pp 229−253.
(57) Gobin, O. C.; Reitmeier, S. J.; Jentys, A.; Lercher, J. A. Comparison of the Transport of Aromatic Compounds in Small and Large MFI Particles. *J. Phys. Chem. C* **2009**, *113*, 20435−20444.
(58) Kortunov, P.; Vasenkov, S.; Chmelik, C.; Kärger, J.; Ruthven, D. M.; Wloch, J. Influence of Defects on the External Crystal Surface on Molecular Uptake into MFI-Type Zeolites. *Chem. Mater.* **2004**, *16*, 3552−3558.
(59) González, G.; Stracke, W.; Lopez, Z.; Keller, U.; Ricker, A.; Reichelt, R. Characterization of Defects and Surface Structures in Microporous Materials by HRTEM, HRSEM, and AFM. *Microsc. Microanal.* **2004**, *10*, 224−235.
(60) Liu, Z.; Fujita, N.; Miyasaka, K.; Han, L.; Stevens, S. M.; Suga, M.; Asahina, S.; Slater, B.; Xiao, C.; Sakamoto, Y.; et al. A Review of Fine Structures of Nanoporous Materials as Evidenced by Microscopic Methods. *Microscopy (Oxford, U. K.)* **2013**, *62*, 109−146.
(61) Lupulescu, A. I.; Rimer, J. D. In Situ Imaging of Silicalite-1 Surface Growth Reveals the Mechanism of Crystallization. *Science* **2014**, *344*, 729−732.
(62) Gobin, O. C.; Reitmeier, S. J.; Jentys, A.; Lercher, J. A. Role of the Surface Modification on the Transport of Hexane Isomers in ZSM-5. *J. Phys. Chem. C* **2011**, *115*, 1171−1179.
(63) Chmelik, C.; Varma, A.; Heinke, L.; Shah, D. B.; Kärger, J.; Kremer, F.; Wilczok, U.; Schmidt, W. Effect of Surface Modification on

Uptake Rates of Isobutane in MFI Crystals: An Infrared Microscopy Study. *Chem. Mater.* **2007**, *19*, 6012−6019.
(64) Tzoulaki, D.; Heinke, L.; Lim, H.; Li, J.; Olson, D.; Caro, J.; Krishna, R.; Chmelik, C.; Kärger, J. Assessing Surface Permeabilities from Transient Guest Profiles in Nanoporous Host Materials. *Angew. Chem., Int. Ed.* **2009**, *48*, 3525−3528.
(65) Heinke, L.; Kärger, J. Correlating Surface Permeability with Intracrystalline Diffusivity in Nanoporous Solids. *Phys. Rev. Lett.* **2011**, *106*, 074501.
(66) Thommes, M.; Mitchell, S.; Pérez-Ramírez, J. Surface and Pore Structure Assessment of Hierarchical MFI Zeolites by Advanced Water and Argon Sorption Studies. *J. Phys. Chem. C* **2012**, *116*, 18816−18823.
(67) Díaz, I.; Kokkoli, E.; Terasaki, O.; Tsapatsis, M. Surface Structure of Zeolite (MFI) Crystals. *Chem. Mater.* **2004**, *16*, 5226−5232.
(68) Yoshida, K.; Sasaki, Y.; Kurata, H. High-Resolution Imaging of Zeolite with Aberration-Corrected Transmission Electron Microscopy. *AIP Adv.* **2013**, *3*, 042113.
(69) Richard, C.; Catlow, A.; D. S. C., Ben Slater, Dewi W. Lewis, Carlos, J.; Pereira, G.. Modeling Nucleation and Growth in Zeolites. In *Handbook of Zeolite Science and Technology*; Auerbach, S. M., Ed.; Marcel Dekker Inc.: New York, 2003.
(70) Slater, B.; Gale, J. D.; Catlow, C. R. A.; Ohsuna, T.; Terasaki, O. Surface Structure Determination of Zeolites. In *Stud. Surf. Sci. Catal.*; E. van Steen, M. C., Callanan, L. H., Eds.; Elsevier, 2004; Vol. *154*, Part B; pp 1197−1203.
(71) Slater, B.; Catlow, C. R. A.; Liu, Z.; Ohsuna, T.; Terasaki, O.; Camblor, M. A. Surface Structure and Crystal Growth of Zeolite Beta C. *Angew. Chem., Int. Ed.* **2002**, *41*, 1235−1237.